Structural and Electrochemical Properties of Newly Synthesized Fe-Substituted MnO_2 Samples

R. Patrice,[†] L. Dupont,[†] L. Aldon,[‡] J.-C. Jumas,[‡] E. Wang,[†,§] and J.-M. Tarascon*[,†]

Université de Picardie Jules Verne, LRCS, CNRS UMR-6007, 33 rue Saint-Leu, 80039 Amiens, France, and Laboratoire des Agrégats Moléculaires et Matériaux Inorganiques, CNRS UMR 5072, Université Montpellier II, Place E. Bataillon, 34095 Montpellier Cedex 5, France

Received January 6, 2004. Revised Manuscript Received April 7, 2004

$Mn_{1-x}Fe_xO_2$ samples, synthesized by a low-temperature process, were characterized for their structural, physical, and electrochemical properties. From X-ray data and EDX analysis in both SEM and HRTEM modes, combined with ^{57}Fe Mössbauer spectroscopy, we gave direct evidence for the first time for a true Fe substitution for Mn up to $x = 0.3$. Beyond such value, the samples are multiphase. The presence of iron was found to affect the electrochemical behavior, with namely the appearance of a second plateau at −0.8 V (vs Hg/HgO) with increasing the iron content at the expense of the one occurring at −0.45 V in the pure MnO_2 phase. We will present evidence, as deduced from both HREM and Mössbauer measurements on reduced samples, that the origin of the −0.8 V plateau could be nested in the electrochemical activity of the $FeMn_2O_4$ phase toward proton in aqueous media.

Introduction

The Zn/MnO_2 alkaline cells have been widely used for the last 50 years, and their interest remains constant due to the increasing demand for reliable portable power sources. Nevertheless, research development efforts are still underway to boost their capacity and enhance their power rate capability. Pursuing such issues in our previous work, we revisited the chemistry of this system and were able to distinguish between two different two-step reduction mechanisms for MnO_2, depending on the nature of the counter electrode, either Pt or Zn. Versus platinum, protons are inserted into MnO_2 over a solid-state reaction until the composition MnOOH, and then Mn^{3+} ions, are released in solution and reduced into Mn^{2+} ions that precipitate as $Mn(OH)_2$. When zinc is used as the counter electrode, 0.5 protons per manganese is inserted over the solid-state reduction. Further reduction would consist of an exchange between inserted H^+ and Zn^{2+} in solution, leading to the formation of electrochemically inactive $ZnMn_2O_4$.[1]

Zn/MnO_2 cells present many advantages such as long shelf life, low cost, or low environmental hazards but are not rechargeable unless we limit the extent of discharge to about one-third of the one-electron capacity, as demonstrated by Kordesh et al.,[2] and exploited by RAYOVAC who commercialized a rechargeable alkaline manganese dioxide (RAM) cell in 1993. During deeper discharge, the ramsdellite structure is irreversibly distorted into a groutite structure to accommodate the insertion of more than 0.5 protons per manganese. Much attention has been aimed toward finding rechargeable MnO_2 that would not need such a discharge limitation. One of the proposed solutions consists of synthesizing substituted manganese oxides. Many authors successfully introduced metals, such as Bi, Pb, Ti, and Cr, into the γ-MnO_2 structure but, to our knowledge, the amounts of dopant reported in the literature, if ever quoted or analyzed, were always limited to a few percent.[3−10]

Besides this possible interest in rechargeable alkaline batteries, the substitution of manganese in γ-MnO_2 would eventually influence its electrochemical properties during the first discharge in primary cells, although we have proven that the voltage of the second electron plateau cannot be adjusted by chemical substitution. Moreover, a new substituted manganese dioxide could eventually find applications in one of the numerous chemistry fields different from electrochemistry such as catalyst or supercapacitors.

Here, we describe the synthesis of a new iron-substituted γ-MnO_2 and give direct experimental evi-

* To whom correspondence should be addressed.
[†] Université de Picardie Jules Verne.
[‡] Université Montpellier II.
[§] Current address: Reston, VA.

(1) Patrice, R.; Gérand, B.; Leriche, J-B.; Seguin, L.; Wang, E.; Moses, R.; Brandt, K.; Tarascon, J.-M. *J. Electrochem. Soc.* **2001**, *148* (5), A448−A455.
(2) Kordesch, K.; Gsellmann, J. Pat. Sch. DE 33 37 568 C2, 1989.
(3) Kainthia, R. C.; Manko, D. J. U.S. Patent No. 5,156,934, 1992.
(4) Bai, L.; Qu, D. Y.; Conway, B. E.; Zhou, Y. H.; Chowdhury, G.; Adams, W. A. *J. Electrochem. Soc.* **1999**, *140*, 884.
(5) Binder, L.; Jantscher, W.; Fiedler, D. A.; Kordesch, K. V. *Electrochem. Soc. Proc.* **1997**, 97−18.
(6) Binder, L.; Jantscher, W.; Hofer, F.; Kothleitner, G. *J. Power Sources* **1998**, *70*, 1.
(7) Urdl, P. Doctoral Thesis, TU Graz, 1994.
(8) Varma, B. P. *Manganese dioxide symposium*, Tokyo; Schumm, Joseph, and Kozawa, Eds; 1981; Vol. 2, p 256.
(9) Nartey, V. K.; Binder, L.; Huber, A. *J. Power Sources* **2000**, *87*, 205.
(10) Laitinen, H. A.; Rajan, K. P. *Manganese dioxide electrode: theory and practice for electrochemical applications* (From the 166th Meeting of The Electrochemical Society, New Orleans, Oct. 8−11, 1984, ECS Proceedings, Vol. 85-4); Schumm, B., Middaugh, R. L., Grotheer, M. P., Hunter, J. C., Ed.; ECS: Pennington, NJ, 1985.

10.1021/cm0401239 CCC: $27.50
Published on Web 06/19/2004

dence for the existence of a solubility range reaching 30%. Furthermore, we will show the influence of iron upon the manganese oxide chemical/physical properties.

Experimental Section

Synthesis. The preparation of iron-substituted γ-MnO_2 powders was derived from the Wang's patent recipe that consists of oxidizing a manganese sulfate solution with sodium peroxodisulfate.[11] Mixtures of $MnSO_4 \cdot H_2O$ and $FeSO_4 \cdot 7H_2O$ with various ratios were dissolved in 100 mL of distilled water to obtain an SO_4^{2-} concentration of 0.84 M. Then, 0.084 mol of $Na_2S_2O_8$ was added to the solutions, which instantaneously turned to orange as the Fe^{2+} is oxidized into Fe^{3+}. While being stirred, the solutions were heated to boiling point for about 5 min, then cooled, and filtered. The resulting precipitates were rinsed three times with distilled water, until the pH rose near 7, and dried for 24 h at 55 °C prior to being characterized. Fe/Mn ratios of 50/50, 20/80, 15/85, 10/90, and 5/95 were tested. Two additional samples were prepared as reference using only manganese or iron sulfate, the former leading to the formation of pure γ-MnO_2 used as the reference phase while the latter gave the natrojarosite phase ($NaFe_3(SO_4)_2(OH)_6$) after 24 h instead of 5 min.

Characterization. All these samples were characterized for their structural, textural, microstructural, chemical, and electrochemical properties. The structural characterizations were performed by means of X-ray diffraction (XRD) with a Scintag diffractometer model PAD V (Cu Kα = 0.15418 nm) or a Siemens D8 diffractometer (Co Kα = 0.179026 nm) equipped with a PSD detector. The latter was used with an Anton Parr 1200 oven for temperature-controlled X-ray diffraction. The morphological studies were carried out by scanning electron microscopy (SEM) with a Philips XL 30 field emission gun (FEG) coupled with energy dispersion spectroscopy (EDS) while the microstructural studies were realized with a high-resolution transmission electron microscope (HR-TEM) Tecnai G^2 F20 STEM (Cs = 1.2 mm, 200 kV, point resolution 0.24 nm, line resolution 0.1 nm) fitted with an EDAX EDS. Thermogravimetric analyses (TGA) were conducted under air using a Setaram TG DTA 92 apparatus with heating ramps of 5 °C/min. ^{57}Fe Mössbauer spectroscopy was conducted at room temperature with a classical EG & G spectrometer in transmission mode using ^{57}Co in an Rh matrix as the γ-ray source. The velocity scale was calibrated from the magnetic sextuplet spectrum of a high-purity iron foil absorber, and the origin of the isomer shift scale was determined from the center of the α-Fe spectrum. The effective thickness of bulk absorbers was in the range of 25−75 mg/cm^2. For the electrochemically reduced samples, the absorbers were the whole electrodes of effective thickness 10 mg/cm^2. The hyperfine parameters δ (isomer shift) and Δ (quadrupole splitting) were determined by fitting Lorentzian lines to the experimental data[12] and by evaluating the hyperfine parameter distribution.[13]

Electrochemical tests were carried out using a three-electrode cell. The positive electrode, which consists of 0.6 g of MCMB 2510 coke, 0.3 g of MCMB 2528 graphite, and 0.2 g of active material, was pressed onto a nickel collector. Two layers of polyamide, soaked in 9 M aqueous KOH electrolyte prepared from reagent-grade KOH pellets dissolved in distilled water, were used as the separator. The positive electrode was impregnated under vacuum to ensure good contact between particles and electrolyte. The counter electrode was made of a platinum wire, and all the potentials were measured versus an Hg/HgO reference electrode. All the electrochemical measurements were performed at room temperature using a Mac-Pile system (Bio-logic S.A., Claix, France) operating in galvanostatic mode.

(11) Wang, E. I.; Bowden, W. L.; Lin, L. U.S. Patent 532,584, 1996.
(12) Rubenbauer, K.; Birchall, T. *Hyperfine Interact.* **1979**, *7*, 125.
(13) LeCaër, G.; Dubois, J. M. *J. Phys. E: Sci. Instrum.* **1979**, *12*, 1083.

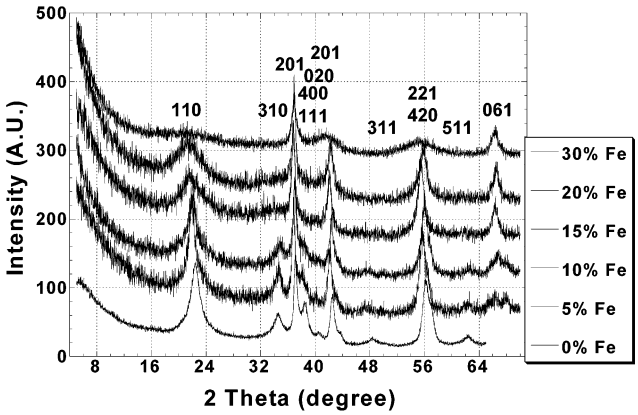

Figure 1. X-ray diffraction patterns of Fe-substituted γ-MnO_2 with various iron amounts (Cu Kα radiation).

Results and Discussion

X-rays Diffraction. The X-ray diffraction patterns of the different Fe-containing samples (0−30 at. % of iron) present large similarities with pure γ-MnO_2 as shown in Figure 1 since there is neither appearance of extra peaks due to second phase nor a shift in the 2θ position of the main Bragg peaks. Therefore, subtle changes are present, namely, an enhancement of the Bragg reflection widths at half-maximum with increasing the iron content, and furthermore a decrease in the peaks intensities except for the peak located at around $2\theta = 67°$. Despite a lack of explanation, Binder et al.[6] observed the same increase in the (061) reflection while enhancing the titanium amount in Ti-doped EMD (electrolytic manganese dioxide). Therefore, the γ-MnO_2 structure seems to be preserved with the introduction of iron but we cannot rule out the possibility of iron precipitation, apart from manganese, as an amorphous iron phase that could not be detected by X-ray diffraction. To test this possibility, we first repeated the synthesis using iron sulfate without manganese sulfate. A yellow precipitate was obtained after the iron sulfate was boiled for 1 night instead of the few minutes necessary to prepare black powders from Fe/Mn solutions. X-ray diffraction of the obtained compound (not shown here) clearly evidenced the formation of well-crystallized natrojarosite $NaFe_3(SO_4)_2(OH)_6$. No peak corresponding to such a phase could be detected during the X-ray diffraction measurements performed on the Fe-substituted MnO_2 samples. This finding tends to favor the substitution of manganese for iron rather than the presence of two phases powders. In this case, the broadening of the peaks could eventually be explained by the presence of defects induced by the substitution of O^{2-} for OH^- to balance the charge difference between Mn^{4+} and Fe^{3+} since a decrease in the average crystallite size would induce a broadening of all the reflections, even the (061) one. However, even in the absence of iron, we should recall that X-ray diffraction patterns of MnO_2 samples are already highly affected by De Wolff defects and microtwinning, both of which can drastically vary from one sample to another. Therefore, any attempts to link the observed peak broadening to the amount of substituted iron will be highly speculative.

Scanning Electron Microscopy and Energy Dispersion Spectroscopy. Scanning electron microscopy coupled with energy dispersion spectroscopy character-

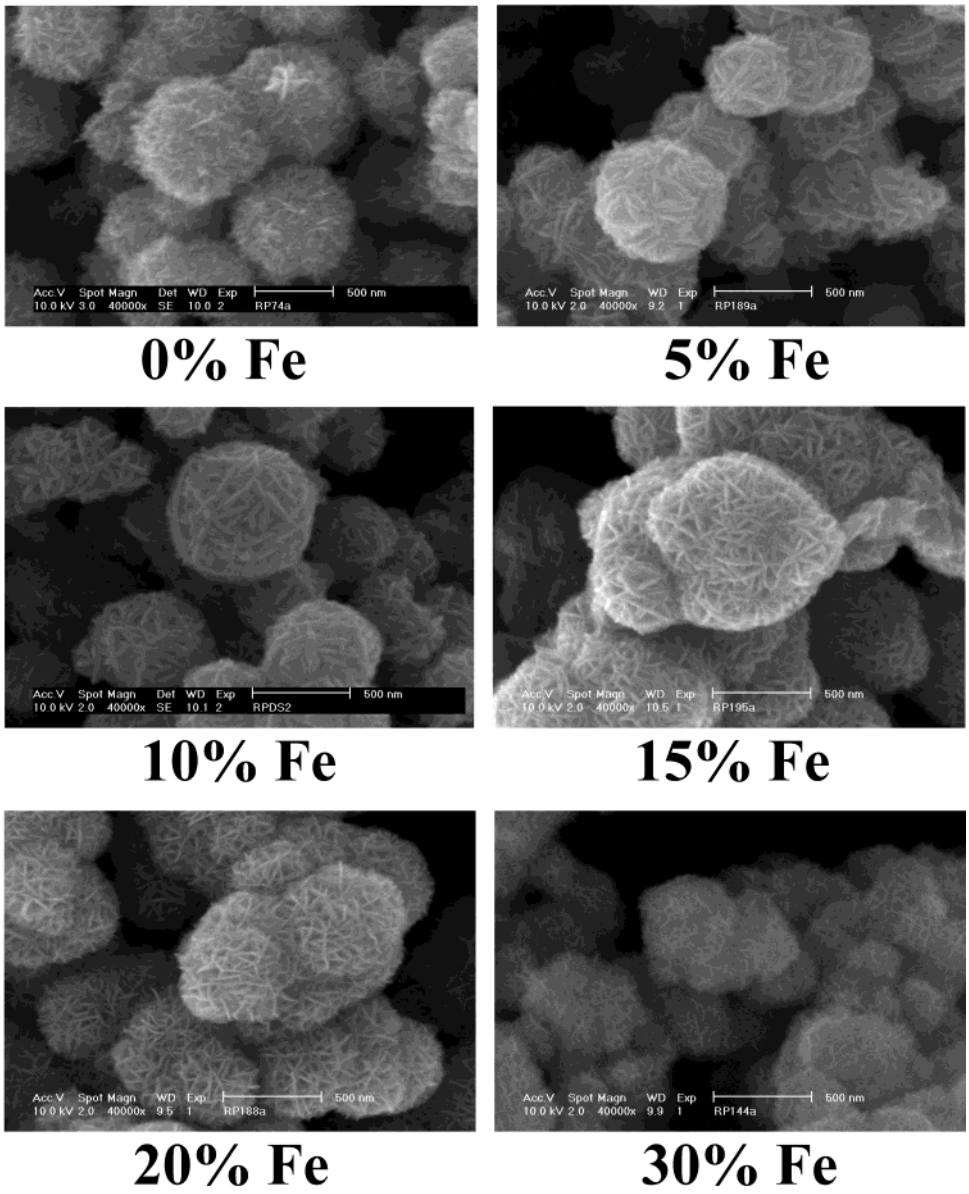

Figure 2. Scanning electron micrographs of Fe-substituted γ-MnO_2 with various iron amounts.

ized all of the obtained powders. Whatever Fe/Mn ratio used, the morphology of the particles remains similar to the one of pure MnO_2 as shown in Figure 2. It consists of 500-nm-diameter spherical particles with irregular surfaces.

The EDS analysis of the different samples indicates the nominal composition except for the 50/50 synthesis, which gives an Fe/Mn molar ratio of 30/70, indicating that the highest Fe/Mn ratio that we can possibly obtain in our substituted series is 30/70 "$Fe_{0.3}Mn_{0.7}O_2$". Iron seems to be homogeneously distributed throughout the sample; however, caution has to be exercised prior to unambiguously claiming the presence of a solid solution "$Fe_{0.3}Mn_{0.7}O_2$" since our experiment was carried out using an SEM microscope having an EDS probe of solely 1 μm in size, thus preventing single-particle investigation. So, overall, the constancy of the Fe-substituted particles morphology with increasing the iron content together with the apparent homogeneous distribution of iron and manganese in the samples, as deduced by SEM measurements, strongly supports the true substitution of Fe for Mn in MnO_2.

Even after the three washings with distillated water, some sulfur remained present in the sample, probably as sulfate, and the EDS measurements indicate about 2% of S for 98% of Mn + Fe.

Thermogravimetric Analyses. Thermogravimetric analyses of the iron−manganese compounds were conducted (Figure 3) and compared to the ones obtained from pure γ-MnO_2. These measurements were coupled with high-temperature X-ray diffraction (Figure 4).

γ-MnO_2 type oxides were extensively studied by thermogravimetry,[14−17] and three important mass losses could generally be observed during heating of these oxides. First, a progressive weight loss from room temperature until 500 °C, which cumulates the departure of adsorbed or weakly bonded water and the

(14) Varma, B. P. *Manganese dioxide symposium*, Tokyo; Schumm, Joseph, and Kozawa, Eds.; 1981; Vol. 2, p 256.
(15) Petit, F.; Lenglet, M.; Arsène, J. *Mater. Res. Bull.* **1993**, *28*, 1093.
(16) Giovanoli, R. *Thermochim. Acta* **1994**, *234*, 303.
(17) Duval, C. *Inorganic Thermogravimetric Analysis*; Elsevier Publishing Company: New York, 1953.

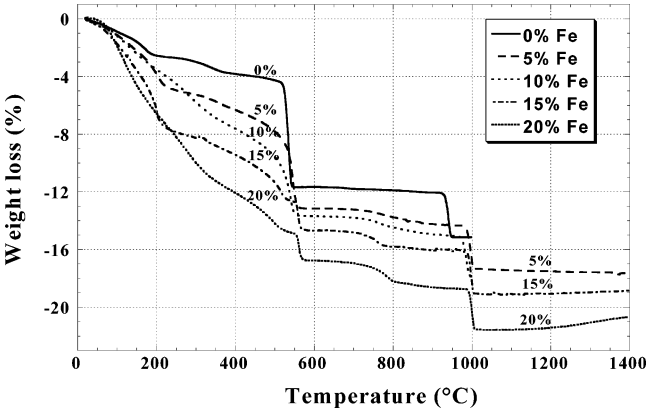

Figure 3. Thermogravimetric analysis of the Fe-substituted MnO_2 with various iron amounts.

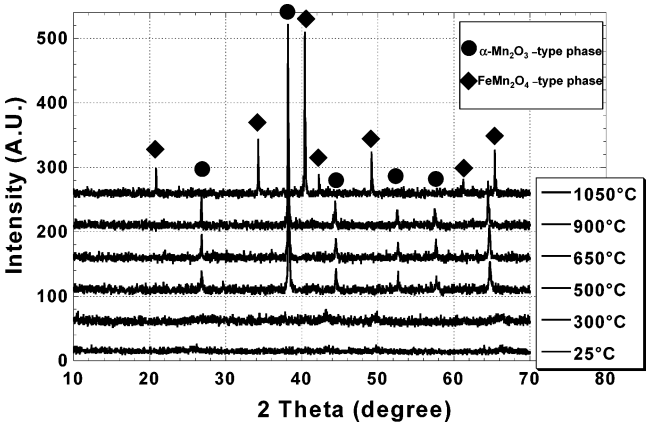

Figure 4. X-ray diffraction patterns of Fe-substituted MnO_2 during heat treatment. (Co Kα radiation).

condensation of hydroxyl groups over the 25−200 °C and 150−500 °C temperature ranges, with the end result being the nucleation of β-MnO_2, respectively. The two following weight losses around 550 and 950 °C correspond to the transformations of MnO_2 into α-Mn_2O_3 and then into Mn_3O_4, respectively. It is also worth noting that, through the $Fe_xMn_{1-x}O_2$, the relative amplitudes of the different weight losses not only vary with the iron content, but with increasing the latter there is also the appearance of a new event on the TGA trace, implying an Fe-driven new phenomenon.

The first loss between 25 and 500 °C becomes more important as the iron/manganese ratio increases. This evolution could be easily explained if one considers that Mn^{4+} is substituted for Fe^{3+} in γ-MnO_2. First, the oxidation state of the two metals being different, the substitution of a manganese atom for iron is expected to lead to the replacement of a surrounding oxygen O^{2-} by an hydroxyl group, OH. Then the amount of hydroxyl groups, and thereby the weight loss associated with it, should proportionally increase with increasing the substituted Fe content, as we observed (Figure 3). Interestingly, such a weight loss does not result in a significant difference between the corresponding X-ray pattern, recorded at 300 °C, and the pattern of the initial compound, with the exception of a very slight increase in the reflections intensities.

As expected, the 550 °C weight loss, due to the transformation of the MnO_2-type compound into Mn_2O_3-type, decreases with the manganese amount in the sample. This phenomenon corresponds to the reduction of Mn^{IV} into Mn^{III} without reaction of the iron.

A new phenomenon appears near 800 °C and grows with the iron content. No structural change can be observed by temperature-controlled X-ray diffraction during this phenomenon since the pattern remains similar to that of α-Mn_2O_3 (Figure 4). Despite a lack of explanation concerning this phenomenon, it seems to be linked to the presence of iron since it does not appear on the thermogravimetric curve of pure γ-MnO_2, and it becomes more important with the iron amount. This weight loss could correspond to the reduction of Fe^{III} into Fe^{II} together with the formation of oxygen vacancies, the weight variation being in good agreement with this supposed oxygen departure. The obtained product would be $Fe_{2x}Mn_{2-2x}O_{3-x}$ with Fe^{II} and Mn^{III} and isostructural to α-Mn_2O_3.

The last loss around 950 °C observed for iron-free γ-MnO_2 is shifted to 1000 °C when the samples contain iron, but always represents about 3% of the initial mass. The final X-ray pattern recorded at 1050 °C corresponds to the $FeMn_2O_4$, one that is similar to that of Fe_3O_4 with displaced reflections. As previously reported by Gillot,[18] the $Mn_{3-x}Fe_xO_4$-type oxides obtained at high temperature undergo a demixion while being cooled. Our samples present the same behavior, leading to the formation of mixtures of $Mn_{3-x}Fe_xO_4$ and Mn_3O_4-type oxides identified by X-ray diffraction (not shown here) when brought back to room temperature.

In short, these preliminary studies of the morphology, structure, and thermal behavior of the iron-containing γ-MnO_2 phases seem to indicate that the precipitated iron atoms replace the manganese one but cannot produce undisputable proof. These techniques do not enable one to describe the iron structural environment in the MnO_2 samples. To throw light on this issue, Mössbauer spectroscopy measurements were conducted, this technique being fully adapted for iron-containing samples.

Mössbauer Spectroscopy. Mössbauer spectroscopy[19,20] is able to give information about the local iron environment, namely, charge distribution, electronic configuration, or valence as well as oxidation state. It could therefore provide valuable information regarding the substitution. ^{57}Fe Mössbauer spectra have been recorded at room temperature for the samples containing 5, 10, 15, 20, and 30 at. % iron (Figure 5).

All the spectra consist of a doublet of Lorentzian lines characterized by an isomeric shift of about 0.37 mm/s and a quadrupole splitting around 0.67 mm/s. These values are characteristic of iron(III) in an octahedral environment. The observed line width (Γ mm/s) is twice the one obtained for α-Fe (0.47−0.57 mm/s instead of 0.26 mm/s). These high values indicate a distribution of the surrounding iron and justify the use of a quadrupole splitting distribution. Therefore, a second adjustment was made following the Le Caër procedure[13] as shown in Figure 6.

γ-MnO_2 is an intergrowth of ramsdellite and pyrolusite structures. To understand the iron environment

(18) Gillot, B.; Laarj, M.; Kacim, S. *J. Mater. Chem.* **1997**, *7*, 827.
(19) Mössbauer, R. L. *Z. Phys.* **1958**, *151*, 124.
(20) Bancroft, G. M. *Mössbauer Spectroscopy, An Introduction for Inorganic Chemists and Geochemists*; Wiley: New York, 1973.

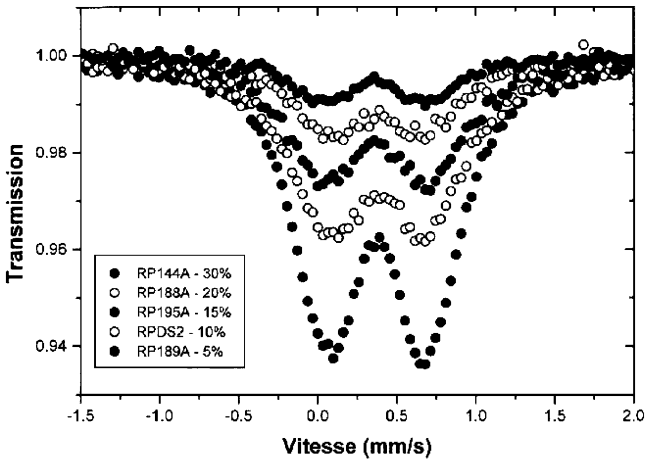

Figure 5. ^{57}Fe Mössbauer spectra of the iron-containing MnO_2 phases.

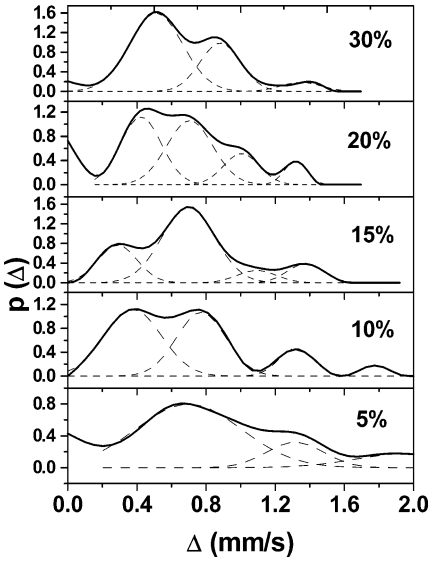

Figure 6. Distribution $p(\Delta)$ of Mössbauer quadrupole splitting obtained from fitting of the spectra (solid straight) for the Fe-substituted (5−30%) MnO_2 with the main contributions represented by Gaussian curves (dotted line).

in γ-MnO_2, we compared the local order between these two structures. Each octahedron is connected to the first eight neighboring octahedra in the pyrolusite form and the first 10 neighboring octahedra in the ramsdellite form. In a statistical repartition, the [MO_6] octahedra are supposed to be occupied by ratios of x iron atoms and $1 - x$ manganese atom. If z is the number of the first neighboring octahedra (8 in pyrolusite and 10 in ramsdellite) and n the number of these octahedra occupied by iron atoms, the probability of finding an environment with n iron atoms as first neighbors is given, for a statistical repartition, by the formula

$$P(x,z,n) = \frac{z!}{n!(n-z)!}x^n(1-x)^{z-n}$$

The probabilities P_n calculated in the cases of pyrolusite and ramsdellite are in good agreement with the various quadripolar splitting values obtained from the Le Caër procedure.

For example, the 15%-Fe sample spectrum is the combination of four quadripolar splittings corresponding to 0, 1 and 2, 3, or 4 neighbors that contribute for 22%, 60%, 7%, and 10%, respectively (Figure 6). In this case, the calculated probabilities to have 0, 1 or 2, 3, and 4 neighbors are 20%, 62%, 13%, and 5% for the pyrolusite and 27%, 62%, 8%, and 2% for the ramsdellite. The comparison between these observations and the theoretical probability calculations finally suggests that the iron atoms are statistically distributed in the prepared samples. They do not precipitate, apart from manganese, but replace the latter in the γ-MnO_2 structure with Fe/Mn ratios ranging from 0 to 3/7.

Electrochemistry. The γ-MnO_2 oxide is widely used as cathode material in alkaline zinc/MnO_2 batteries. In such cells, manganese oxide first undergoes a solid-state reduction from MnO_2 to MnOOH followed by an occasional dissolution−reduction−precipitation mechanism leading to the formation of $Mn(OH)_2$.[1] It was therefore interesting to test the iron-substituted γ-MnO_2 samples for their electrochemical behaviors in a KOH medium.

These oxides were reduced using a C/10 rate (e.g., reaction of 1 proton in 10 h) and compared to pure γ-MnO_2 prepared using the same synthesis route (Figure 7). The voltage−composition curve of pure γ-MnO_2 first presents a sloping profile during the solid-state reduction followed by a plateau corresponding to the reduction of Mn^{3+} in solution. It is important to note that the overall reduction capacity generally observed for γ-MnO_2 in alkaline cells is limited to about 1.6 electrons per manganese, equally parted between solid state and via solution reductions reactions.

For the substituted samples, the voltage−composition curves profiles depend on the iron amounts, especially for the second part of the curve. The first part of the reduction curves presents a slight stabilization around −0.25 V corresponding to the composition of the groutellite ($H_{0.5}MnO_2$), which is the transition form from the ramsdellite structure to the groutite one. Nevertheless, the overall capacity of the first electron discharge remains constant at around 0.8 electrons per metal atom despite the presence of 5−20% of iron.

During the second part of the reduction and while the iron amount is increased, one could note a decrease in the capacity corresponding to the plateau around −0.45 V together with the appearance and lengthening of a second plateau at −0.8 V. The variations of the capacities associated with these two plateaus cannot be solely explained by the substitution of manganese for iron. The capacity of the first plateau decreases faster than the manganese amount and totally disappears with the replacement of only one-third of the manganese atoms, indicating that the presence of iron indirectly prevents the manganese reduction via the known in-solution way. In the meantime, the second plateau capacity increases twice as fast as the iron amount. During reduction, all the iron−manganese oxides, with formula $Fe_xMn_{1-x}O_2$, show a second plateau having a capacity of $2x$ electrons; that is, we observe the reaction of 2 electrons for each iron atom. At first sight, since such a plateau does not appear with pure γ-MnO_2, it would be tempting to ascribe its origin to the $Fe^{3+} \rightarrow Fe^{2+}$ redox couple. However, this does not hold since the observed capacity is higher than 1 electron per iron atom. Furthermore, the reduction of Fe^{3+} to Fe^0, which could account for

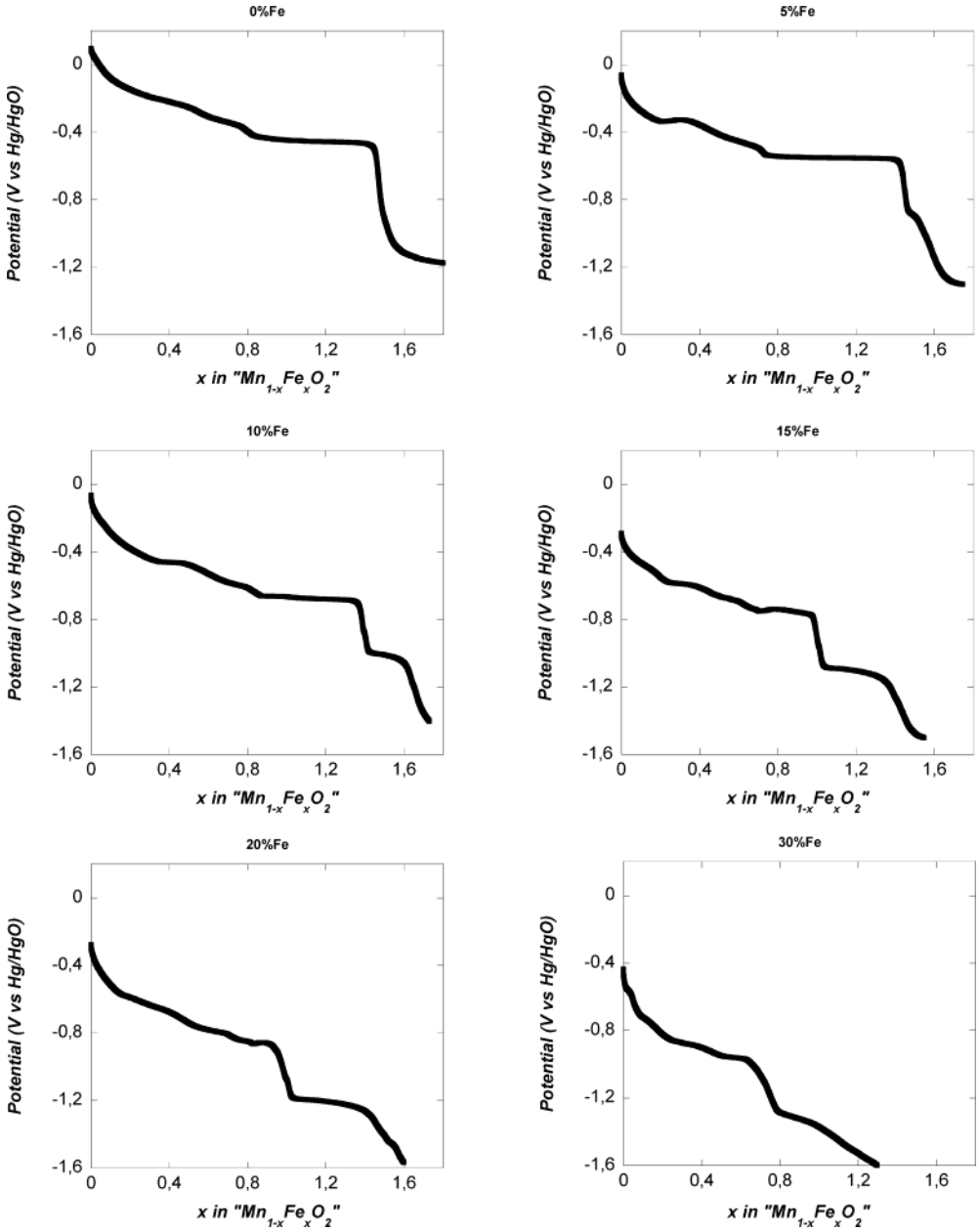

Figure 7. Electrochemical curves of the reduction of the iron-containing MnO_2 phases at room temperature using a C/10 rate (1 proton in 10 h).

some of the observed extra electrons, is quite unlikely. Thus, to obtain more insight into this issue, the 20% iron sample reduction was followed by Mössbauer spectroscopy at various depths of discharge, namely, 0.6 e^-/Mn (−0.3 V), 0.9 e^-/Mn (−0.5 V), and 1.6 e^-/Mn (−1.2 V). Once reduced, these samples were washed three times with distillated water and dried for 24 h at 50 °C. No drastic changes of the recorded spectra were observed and particularly no presence of metallic iron nor Fe^{2+}. The total electrochemical capacity is therefore attributed to the reduction of manganese via processes influenced by the presence of iron.

Despite the decrease in the manganese amount in the $Fe_xMn_{1-x}O_2$ samples, the overall capacity remains almost constant, except for the 30% iron one where the capacity is of 1.4 electrons per formula unit. Then, as the iron amount is increased, the reduction yield of the manganese is increased, and for the 20% and 30% iron phases all the manganese atoms are reduced until the +2 oxidation state.

Finally, the presence of iron in the samples changes the electrochemical characteristics of the γ-MnO_2 phases but we are not yet able to clearly explain the −0.8 V reduction mechanism. Nevertheless, we noted that one iron atom implies the Mn^{3+}/Mn^{2+} reduction of two manganese atoms over the −0.8 V plateau, indicating the possible formation of a "$Fe^{3+}Mn^{2+}{}_2O_xH_y$"-type phase during the reduction.

To throw some light on the −0.8 V phenomenon, we performed a high-resolution transmission electron microscopy (HRTEM) study on the 20% iron sample reduced until −0.75 V, that is, just before the −0.8 V plateau, to identify the phase responsible for this plateau, and which could be formed during the first part of the reduction.

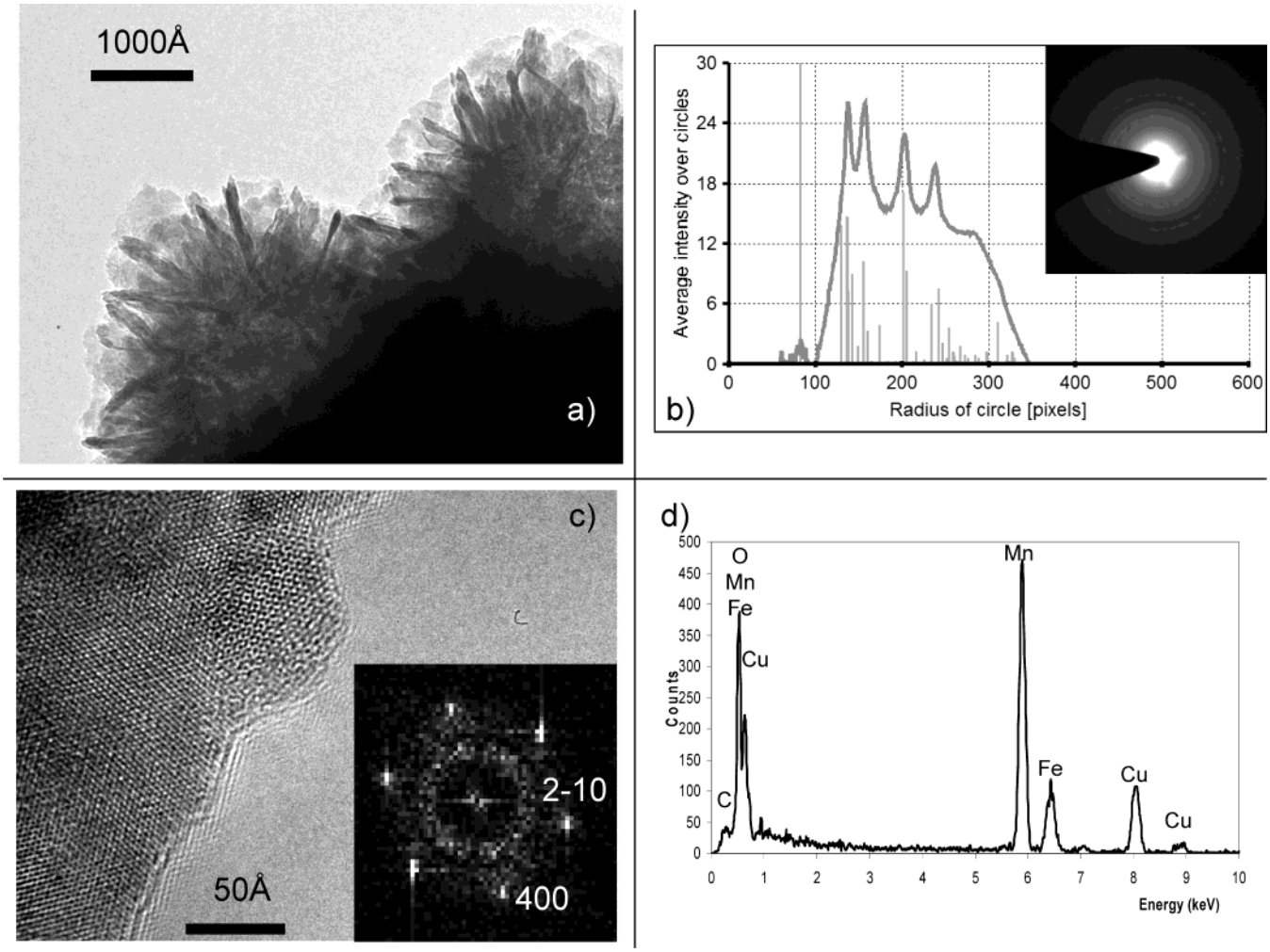

Figure 8. TEM study of the 20% iron substituted manganese dioxide. (a) Bright field image of the agglomerates. (b) XRD-like distribution obtained from the corresponding SAED pattern, given in the inset, treated with process diffraction software. (c) HRTEM image realized on the edge of a particle. The corresponding FFT, given in the inset, is indexed with ramsdellite-type cell parameters. (d) EDS spectrum recorded on the same studied region.

TEM Studies. *(a) Study of the Initial 20% Iron Substituted Manganese Dioxide Sample.* According to the bright field image presented in Figure 8a, the sample is made of spherical agglomerates of thin platelets having a diameter of several thousands of angstroms. The selected area electron diffraction (SAED) pattern realized on an aggregate could not be easily indexed with the ramsdellite-cell parameters. Indeed, as shown in Figure 8b, the indexation of the XRD-like distribution obtained by treatment of the SAED pattern (inset) through Process Diffraction software[21] is quite hazardous. Not all of the numerous ramsdellite reflections are clearly observed, the weakest being lost in the background. To determine the real structure and composition of the material, a combined HRTEM/EDS study was undertaken. A recorded HRTEM image of the edge of one of the platelets is given as an example in Figure 8c. The image contrast is made of white dots having a hexagonal symmetry. Changes in the contrast allow determination of the crystallite size that ranges between 50 and 100 Å. A fast Fourier transform (FFT) realized on the image is presented in the inset. According to this specific FFT that corresponds to a *c** zone axis, and for all of the others obtained during this study, the punctual dots could be indexed using the ramsdellite cell parameters. Finally, using the FEG TEM microprobe (whose diameter size could be estimated at 20 Å), the substitution process could be demonstrated as shown on the EDS spectrum (Figure 8d). Indeed, the iron peak is clearly observed, and according to the quantitative EDS analysis the nominal 20/80 iron-to-manganese ratio is preserved within the particles.

(b) TEM Study of the Reduced Sample. Once reduced to −0.75 V, the 20% iron compound was recovered by centrifugation, rinsed three times, and dried at 50 °C.

Bright Field Image and EDS Analysis. The observation of the reduced phase by HRTEM shows three types of particles (Figure 9a). Carbon microbeads are either visually identified owing to their morphology or by EDS spectroscopy. The two other types of particles are large platelets and shapeless small particles, respectively. In a first approximation, the real existence of the small particles could be suspected: Indeed, these particles could be considered as crumbs from the large platelets. Nevertheless, the EDS analyses realized on both large and small particles evidence a drastic change in the material composition. As shown in Figure 9b, the amount of iron is higher in the small particles than in

(21) Lábár, J. L. *Microsc. Anal.* **2002**, *75*, 9−11.
(22) Mactempas: http://www.totalresolution.com/MacTempas.html.

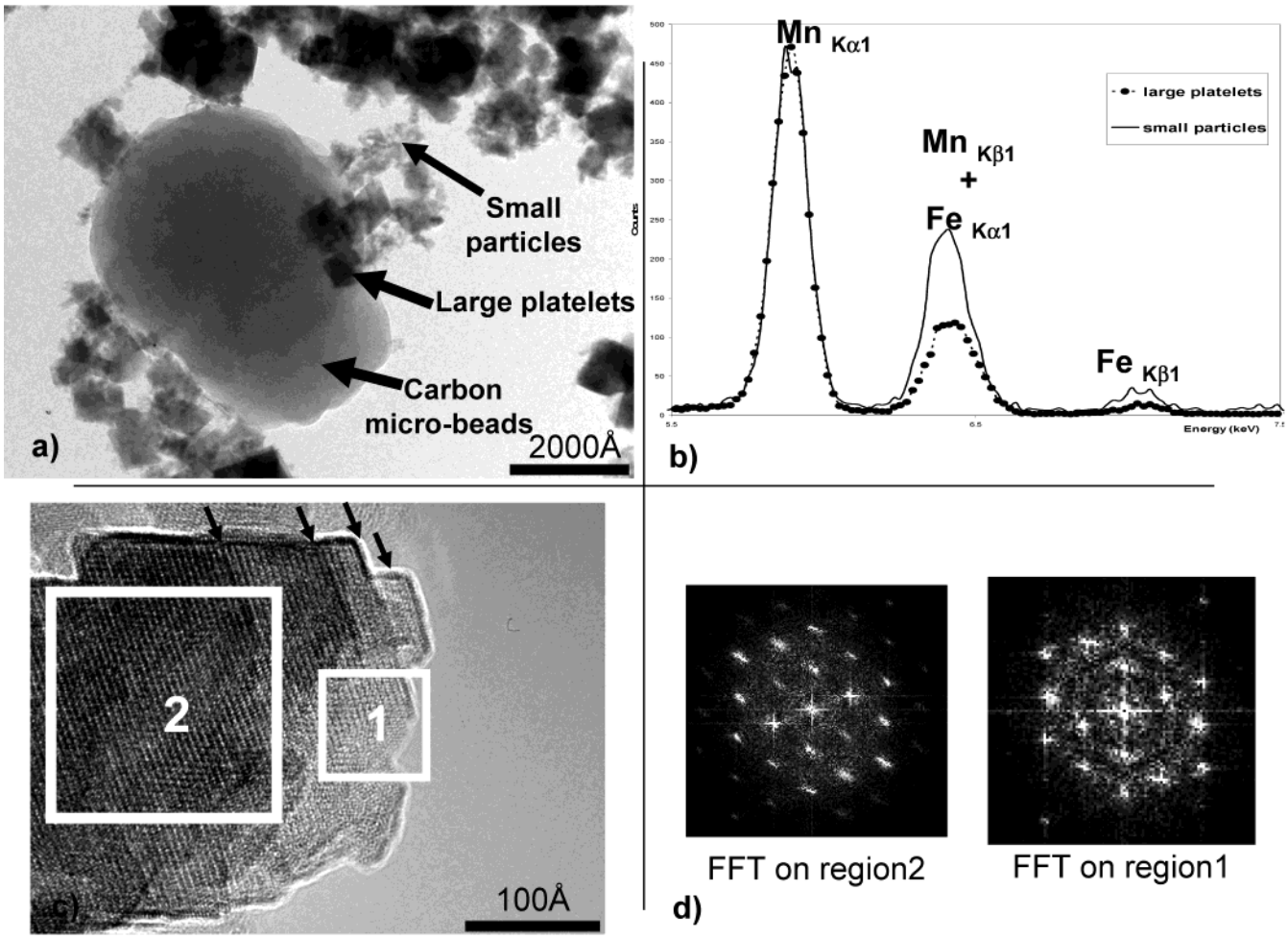

Figure 9. TEM study of the cycled and washed material. (a) Bright field image of the composite material showing carbon balls and two types of particles: large platelets and small particles. (b) EDS spectra recorded on both small and large particles showing that the composition differs. (c) HRTEM image realized on large platelets; the black arrows delimit the matter layers giving a puff aspect to the particle. Two regions, namely, 1 and 2, were chosen to realize FFT presented in (d).

the large platelets. According to quantitative EDS analyses, the composition of the large platelets is quite similar to that of the initial material (manganese/iron ratio equal to 80/20) while the small particle composition is closer to two manganese atoms per one iron atom (66.7/33.3). This result proves that the two types of particles could be considered as coming from two distinct phases that remain to be identified.

According to our background in the field of alkaline batteries, the large platelets are probably made of an iron-substituted Mn_3O_4-type phase probably obtained during the washing of the sample. Indeed, it is well-known that $Mn(OH)_2$ is unstable in water since dissolved O_2 immediately oxidizes it into Mn_3O_4. We previously showed that when this reaction occurs in the presence of a transition metal ion M^{n+} in solution, it could easily lead to the formation of a mixed oxide with Mn_3O_4 structure. For example, the oxidation of $Mn(OH)_2$ in a Zn^{2+} solution led to the formation of $ZnMn_2O_4$.

During the reduction of our sample, the plateau around −0.4 V corresponds to the reduction of MnOOH into $Mn(OH)_2$. The cell used for the tests does not prevent contact between air and the electrolyte. Dissolved oxygen in the electrolyte or in the water used to wash the sample can therefore oxidize $Mn(OH)_2$ in the presence of iron, leading to the formation of the iron−

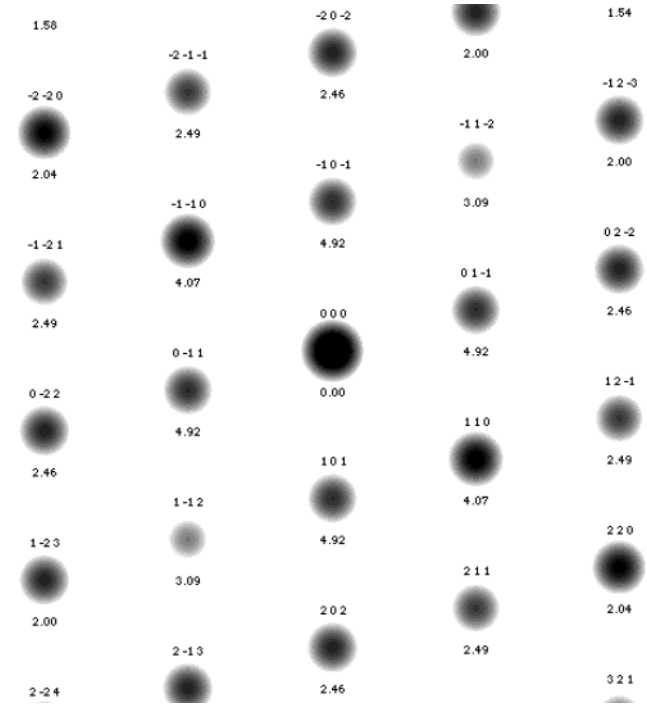

Figure 10. Simulated SAED pattern of an Mn_3O_4 phase along the $[\bar{1}11]^*$ zone axis. The *hkl* indexing and *d* distance are given above and below each spot, respectively.

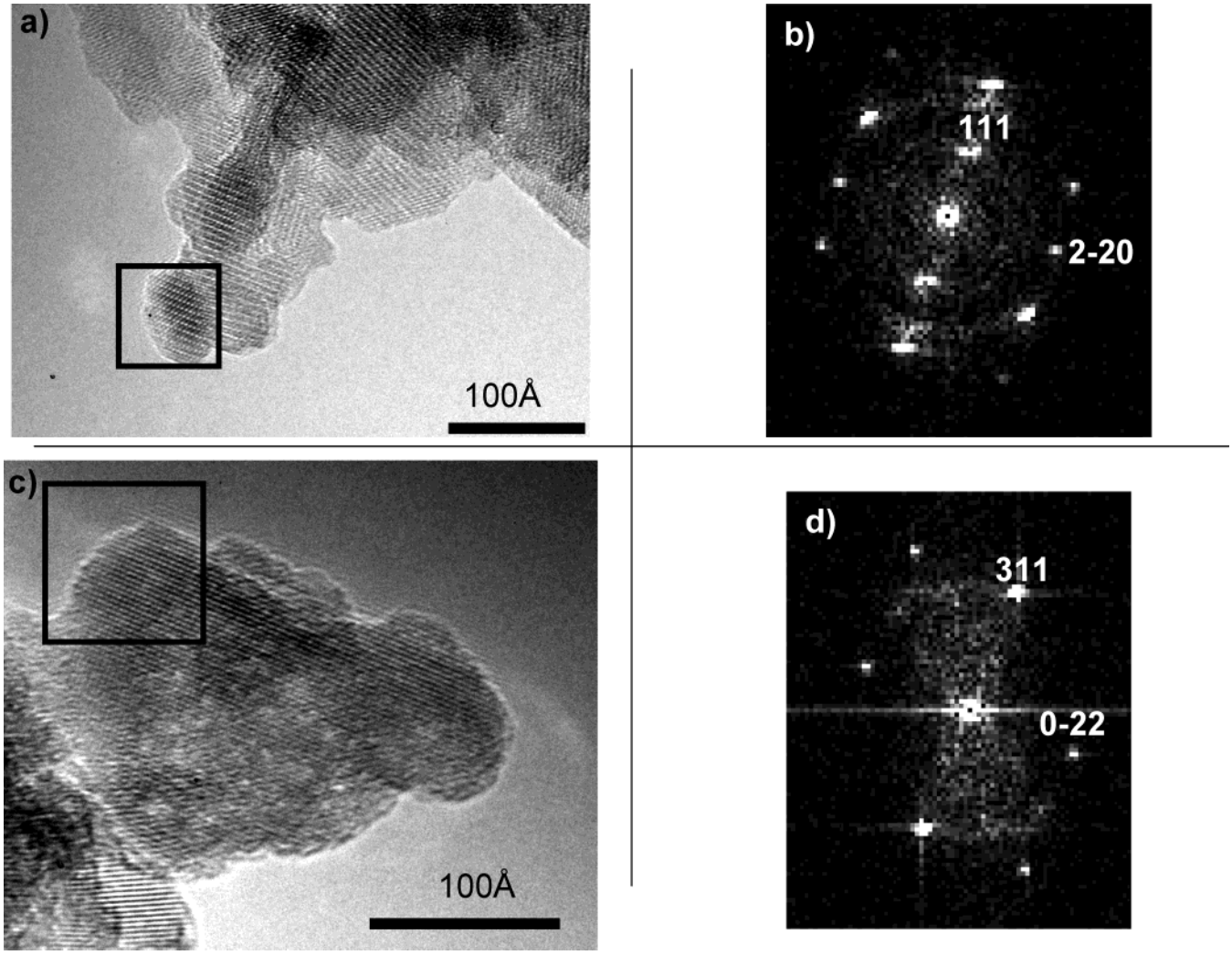

Figure 11. HRTEM study of the small particles. (a) and (c) images with the selected regions used to calculate the FFTs presented in (b) and (d), respectively. Each FFT is indexed using the $FeMn_2O_4$-type cell parameters.

manganese oxide having the Mn_3O_4 structure. This oxide presents the same platelet morphology as the $Mn(OH)_2$ previously obtained from the reduction of MnO_2 vs platinum.[1]

According to EDS analysis, the small platelets could correspond to $FeMn_2O_4$. Owing to the small quantity of such particles within the sample, it turned out to be very difficult to prove the existence of this phase by means of classical techniques such as XRD. Only an HRTEM study would enable demonstration of the structural origin of both large and small particles.

HRTEM Study. (1) Large Platelets. An HRTEM image realized on a large platelet is given as an example in Figure 9c. The puff nature of the particle is nicely observed with the superposition of independent material sheets, whose growth edges are pointed out by arrows. To determine the origin of this platelet from a crystallographic point of view, two FFTs (Figure 9d) were realized from the selected regions 1 and 2, delimited by white squares (Figure 9c), corresponding to a thin and a thick part of the particle, respectively. According to the hypothesis given above, the Mn_3O_4 and $FeMn_2O_4$ cell parameters were tested to index the spots on the FFTs. The two structures having close relationships, it is quite difficult to choose between the two types of cells. Indeed, if the space groups are not taken into account, the FFTs could be indexed with both structures leading to a $[\bar{1}11]^*$ zone axis for Mn_3O_4 cell parameters and a $[\bar{1}10]^*$ zone axis for the $FeMn_2O_4$ cell parameters. Nevertheless, since we have a direct and an inverse spinel, the *hkl* reflections conditions induced by the space group combined with the dynamical behavior of the electrons allowed choosing between the two phases. Electron diffraction patterns simulations were realized with the MacTempas software[22] for both phases and zone axis, and considering two crystals' thickness: 20 and 100 Å. According to the obtained simulations, only the Mn_3O_4 cell parameters induce simulations along the $[\bar{1}11]^*$ zone axis, fitting perfectly the experimental FFTs presented in Figure 9d. The simulated pattern calculated for a thickness of 100 Å is given with the *hkl* indexing and *d* spacing in Figure 10 and could be correlated to the FFT region 2 of Figure 9d.

According to this study, we can conclude that the large platelets are made of 20% iron substituted Mn_3O_4-type phase with the supposed formula $Fe_{0.6}Mn_{2.4}O_4$.

(2) Small Particles. The same approach was undertaken to determine the nature of the small particles. The work was quite easier since these particles having no specific shape lied on several different planes. Consequently, various zone axes were determined from FFTs of the recorded HRTEM images. Two of them are

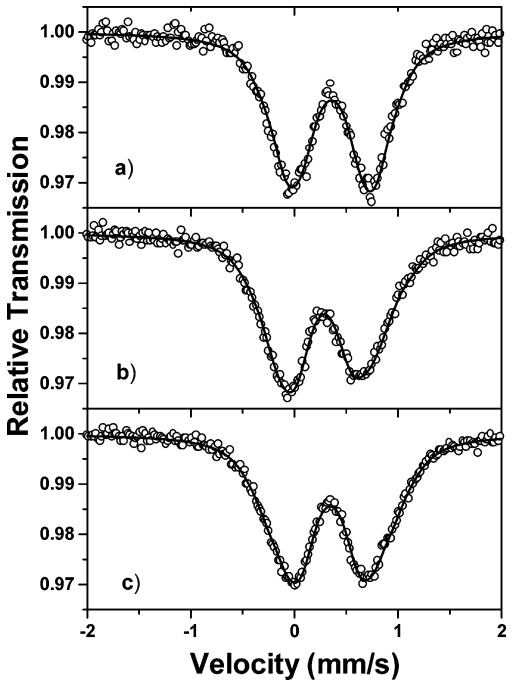

Figure 12. ^{57}Fe Mössbauer spectra of Fe-substituted (20%) MnO_2 recorded at different depths of electrochemical reduction: (a) −0.325 V, (b) −0.600 V, and (c) −1.16 V.

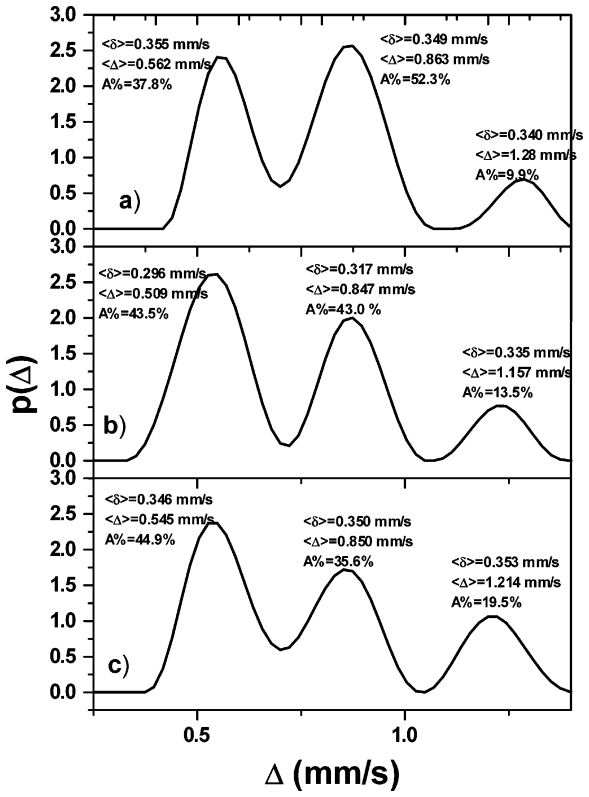

Figure 13. Distribution $p(\Delta)$ of Mössbauer quadrupole splitting obtained from fitting of the spectra relative to Fe-substituted (20%) MnO_2 recorded at different depths of electrochemical reduction: (a) −0.325 V, (b) −0.600 V, and (c) −1.16 V.

given as examples in Figure 11. The FFTs presented in Figure 11b,d were calculated from the square region of the HRTEM images (Figure 11a,c, respectively). In both cases, and generally for all the FFTs calculated during this study, only $FeMn_2O_4$-type cell parameters allowed indexing of the reflections spots. The FFTs in parts (b) and (d) of Figure 11 correspond to $[11\bar{2}]^*$ and $[2\bar{3}\bar{3}]^*$ zone axes, respectively. We can conclude from this study that the small particles are made of the $FeMn_2O_4$ phase.

Interestingly, by exploiting the Mössbauer data recorded during the reduction of the 20% iron sample (Figure 12), we can deduce valuable information regarding the reduction process. First, whatever stages of the reduction process (−0.325, −0.600, −1.2 V), the measured isomeric shifts remain constant, implying that iron remains in the +3 oxidation state upon reduction. Second, owing to the dependence of the ^{57}Fe quadripolar splitting as a function of the charge repartition, it is possible, as discussed later, to distinguish between Fe^{III} and Mn^{IV} or Mn^{II} sites repartition. In contrast, it is much more difficult to distinguish between Fe^{III} and Mn^{III}.

Fitting of the spectra with a quadrupole splitting distribution[13] clearly shows the appearance of a third component ($\delta \sim 0.35$ mm/s and $\Delta \sim 1.16-1.28$ mm/s), whose contribution increases during the reduction (Figure 13). This component with a large quadrupole splitting value can be attributed to an asymmetric charge repartition including Fe^{3+}, Mn^{3+}, and Mn^{2+}. Its contribution is at its maximum at the end of the reduction (Figure 13c).

Using a calculation similar to the one previously presented for the starting materials, but applied to a spinel structure, we were able to calculate the $P(x,z,n)$ probabilities with x being the Fe^{3+} cation content, $1 - x$ the Mn^{2+} cation content, z the number of neighboring sites (6 for spinel) and n the number of neighboring Fe^{3+} cations. For the spinel $Fe_{0.6}Mn_{2.4}O_4$ (large platelets) the calculated probabilities for the $P_0 + P_1$, $P_2 + P_3$, and $P_4 + P_5$ configurations are 42%, 51%, and 7%, respectively. In the case of the spinel $FeMn_2O_4$, the same calculation leads to 11%, 54%, and 35%.

For the sample reduced until $x = 0.45$, the comparison between the calculated probabilities and the contributions determined from the experimental spectra (Figure 13a) are in agreement with the formation of $Fe_{0.6}Mn_{2.4}O_4$ spinel and a statistical repartition of Fe^{3+} cations on octahedral sites. For the sample reduced until $x = 0.95$ (Figure 13b) all the Mn^{4+} have been reduced into Mn^{3+}, and some of the as-formed Mn^{3+} are already reduced into Mn^{2+}. The increasing contribution of the third component can be explained by the appearance of the $FeMn_2O_4$ inverse spinel, which is characteristic of the small particles. This sample-type segregation will continue upon reduction until a structural phase transition to a spinel phase can occur. As a matter of fact, the Mössbauer spectra of the fully reduced sample (Figure 13c) confirm this point. Indeed, iron stays in the +3 oxidation state, and only manganese atoms are reduced. One can suppose that Mn^{2+} occupies the tetrahedral sites of the spinel and that iron stands in octahedral sites. For the fully reduced sample the contributions determined from the experimental spectrum (45%, 36%, and 19%) account for the presence of both spinel compositions $Fe_{0.6}Mn_{2.4}O_4$ and $FeMn_2O_4$ in agreement with the spinel model, further supporting the observations previously made by HRTEM.

Conclusion

During this study, we were able to synthesize a new iron-substituted γ-MnO_2 series whose domain of existence ranges from 0 to 30%. The substitution has been proven by means of a Mössbauer study that clearly evidenced the statistical distribution of the iron atoms in the manganese oxide. The structural and textural characteristics of these samples remain similar to the ones of pure γ-MnO_2 but the electrochemical properties are affected by the presence of iron. HRTEM studies as well as Mössbauer enabled us to throw some light on the reduction mechanism in alkaline media. Up to 0.75 V, these iron-containing samples seem to be reduced into two types of phases: an $FeMn_2O_4$-type phase and an $Mn(OH)_2$-type phase that transforms into an Mn_3O_4-type phase during the washing of the recovered samples.

While this new Fe-substituted MnO_2 series does not present attractive electrochemical properties in alkali media with respect to pure $Mn0_2$ phases, it could present some positive attributes for supercapacitors applications, as we are just beginning to experience.

CM0401239